
Article:
Su, J, Li, K orcid.org/0000-0001-6657-0522, Li, Y et al. (2 more authors) (2022) A Novel State-of-Charge-Based Droop Control for Battery Energy Storage Systems to Support Coordinated Operation of DC Microgrids. IEEE Journal of Emerging and Selected Topics in Power Electronics, 11 (1). pp. 312-324. ISSN 2168-6785

https://doi.org/10.1109/JESTPE.2022.3149398

Design and management of power electronics interfaced energy storage system

A Novel State-of-Charge-Based Droop Control for Battery Energy Storage Systems to Support Coordinated Operation of DC Microgrids

Jialei SU, Kang LI, *Senior member, IEEE* , Yongfei LI, Chen XING,

James YU

***Abstract*—A modern DC microgrid often comprises renewable energy sources (RESs) such as Photovoltaic (PV) generation units, battery energy storage systems (BESSs), and local load, and it is also connected to the utility grid through a point of common coupling (PCC). While most existing approaches have to rely on communication links to achieve desirable control performance, this paper proposes a novel control strategy without resorting to the communication links. This is achieved by assigning BESSs as master units and regulating the DC bus voltage with a novel state-of-charge (SoC)-based droop control, where the BESSs coordinate the slave units (e.g. RES, utility grid) with the aid of the DC bus signaling (DBS) technique to avoid overcharging and over-discharging of these BESSs. In the proposed droop control, the reference voltage for these BESSs is designed for coordinated operation between BESSs and utility grid, it is maintained constant in normal SoC range, which can reduce DC voltage variation. Droop coefficients designed for SoC balance of BESS are dynamically adjusted based on their own SoC values. Furthermore, the preset maximum deviation between the reference voltage and DC bus voltage ensures reliable coordinated operation. Real-time hardware-in-loop (HIL) experiments considering three different scenarios are conducted to validate the effectiveness of the propose method.**

I. Introduction

The growing demands for electricity, compounded by the pressing need for decarbonization, is driving the rapid global transition of the electrical power systems [1]. Amongst a wide range of novel power system technologies proposed so far, the concept of microgrids is prominent [2]. A microgrid can be AC- or DC-based and the latter is now drawing substantial interests in recent years due to its distinctive features, such as no need for frequency control [3] and harmonics cancellation [4], the absence of reactive power [5] and no requirement for synchronization [6]. Further, the need for DC coupling of most renewable sourced generators and battery energy storage systems (BESSs) together with increasing DC power demand from electric vehicles (EVs), has put the DC microgrid as a trend in developing future distribution systems [7, 8]. As illustrated in Fig.1, a typical DC microgrid for EV fast-charging may include renewable energy sources (RESs), BESSs, and is connected to the utility grid through the point of common coupling (PCC).

The control objectives of the DC microgrids include keeping the DC bus voltage within its designed range, maintaining the state-of-charge (SoC) of all the BESSs within their acceptable limits, and avoiding BESS overcharging or over-discharging; and balancing the SoCs of different BESSs [9]. Additional targets may include maximizing the utilization of the RES generated power, and ensuring high efficiency and reliability.

However, due to the stochastic and intermittent natures of RESs and ever-surging time-varying loads imposed on the DC microgrid, there exist great challenges to meet these control objectives [10].

The control strategies for a DC microgrid can be categorized as centralized or decentralized [11]. In centralized control, a microgrid central controller (MGCC) monitors the entire system through an external communication link and dispatches the sources and loads according to the designed control objectives. Hence, the centralized control introduces a high computation burden on the MGCC. In addition, the MGCC needs to be reprogrammed when new sources or loads are introduced. Centralized control may suffer from single-point-failure issues because of heavy dependence on the MGCC, which reduces the system flexibility and reliability [12-14].

Decentralized control overcomes these shortcomings by making decisions based only on the local information, droop control is a typical decentralized control and widely used in DC microgrids [15]. In this scheme the deviation between the reference voltage and actual DC bus voltage is used for automatic power-sharing between paralleled converters. As discussed earlier, one of the key control targets for the DC microgrid with BESSs is the SoC balancing, and SoC information is often incorporated into the droop control law. For example, adaptive droop control is adopted in [16] and [17] to change the droop coefficients based on the SoCs of the BESSs, where in the charging mode, droop coefficients are proportional to the n-th order of the SoC, while in the discharging mode, droop coefficients are inversely proportional to the n-th order of the SoC. References [18] and [19] proposed to change the droop coefficients based on the difference of the SoCs of BESSs and the preset reference SoC value. The SoC-based droop controls in these approached [16]-[19] do not rely on the communication links between different BESSs, and BESSs at low SoC level absorb more power while discharge less power by adopting a SoC-dependent droop coefficient, and vice versa. An SoC-based current sharing method is proposed in [20], where SoCs are balanced by comparing the preset maximum SoC value with the actual SoCs of BESSs in the discharging mode, while comparing the preset minimum SoC value with the SoCs of BESSs in the charging mode. Like the approaches in [16]-[19], this method also does not rely on the communication links. Zhi et al proposed an SoC-based virtual DC machine (VDCM) control strategy for BESSs, where the transient stability of DC bus voltage is enhanced using the output inertia of VDCM and SoCs are balanced by comparing the SoCs of BESSs with the average SoC [21]. Zeng et al [19] also proposed to balance the SoCs by comparing the SoCs of BESSs with the average SoC,

while three different parameters are used to achieve desirable balancing speed and for accurate regulation [19]. Zhang et al [22] also used the average SoC information to ensure that the SoC equilibrium is reached quickly [22]. In [19, 21, 22], the communication between BESSs is required to calculate the average SoC. While Lee et al [23] proposed a SoC-based droop control, which is based on the battery cycle life curve comprising the battery degradation information, and an equal incremental cost point for BESSs is calculated. As an energy buffer, BESSs can also act as master units and regulate the DC bus voltage, furthermore, they can coordinate with other slave sources (e.g. RES and utility grid) with the assistance of the DC bus signaling (DBS) technique. The slave power sources change their operation modes according to the DC bus voltage which is dependent on the SoCs of BESSs. DBS uses the DC bus as a communication line, which ensures normal operation of the DC microgrid even under communication failure or non-communication conditions [24]. Wu et al use a BESS to regulate DC bus voltage according to its SoC value, and RES power curtailment or load shedding decision is made according to DC bus voltage, hence, the BESS avoid overcharging and over-discharging [25]. Based on the DC bus voltage and SoC of the BESS, a decentralized control strategy is proposed in [26] to achieve coordinated operation between a photovoltaic (PV) panel, the grid. However, in these two papers, only one BESS is considered, and these schemes lack the coordination between different BESSs, such as power-sharing and SoC balance strategies. Therefore, the SoC-based droop control with SoC balance capability while combing DBS method can address this issue, and the combination of these two methods has not yet been fully researched. Authors in [27] and [28] use SoC-based droop control for BESSs to coordinate RES and utility grid, where the reference voltages for different BESSs follow the changes in their corresponding SoCs across full SoC ranges, and SoC are balanced with different reference voltages. However, SoC dependent DC bus voltage regulation across the full SoC range may cause large DC bus voltage variations. Furthermore, in [27], the coordinated operation between utility grid and BESSs are not addressed, while in [28], the PV is switched from maximum power point tracking (MPPT) into constant voltage mode to reduce power generation when the SoCs of the BESSs are high, but this suppresses fully utilization of renewable source generated power.

To address the drawbacks, this paper proposes a novel SoC-based droop control for the parallel connected BESSs. With proposed droop control, BESSs act as master units and regulate DC bus voltage, and BESSs coordinate the slave units (e.g. RES, utility grid) to avoid overcharging and over-discharging with the aid of

the DBS method. In the proposed droop control, the reference voltage is designed for coordinated operation between BESSs and utility grid, it is maintained constant in normal SoC range, unless the BESS reaches its low SoC limit or lies in the high SoC range, hence, DC bus voltage variation is significantly reduced; droop coefficients are designed for SoC balance, they are dynamically adjusted based on their own SoC values of BESSs. Furthermore, the preset maximum deviation between the reference voltage and DC bus voltage ensures the reliable coordinated operation between BESSs and utility grid. That BESSs act as master units helps RES generates maximum power and DC microgrid work autonomously (in islanded mode) in most of time without relying on communication link. Lastly, since the proposed droop controller is current source-based, the droop coefficients do not affect power-sharing accuracy, hence when determining droop coefficients it does not have a trade-off between voltage regulation and power-sharing accuracy like many conventional methods.

The remainder of this paper is organized as follows. Section II first presents a brief introduction of the DC microgrid and the proposed droop control is given in details. Then, the SoC balancing based on the proposed droop control is investigated under five different scenarios. The constraints on the ranges of the control parameters are also analyzed. Section III details the coordinated operations of all elements in the DC microgrid using DBS. Section IV presents the the stability analysis of DC microgrid with the proposed droop control, while the results of hardware-in-loop (HIL) experiments and analysis are given in Section V. Finally, Section VI concludes the paper.

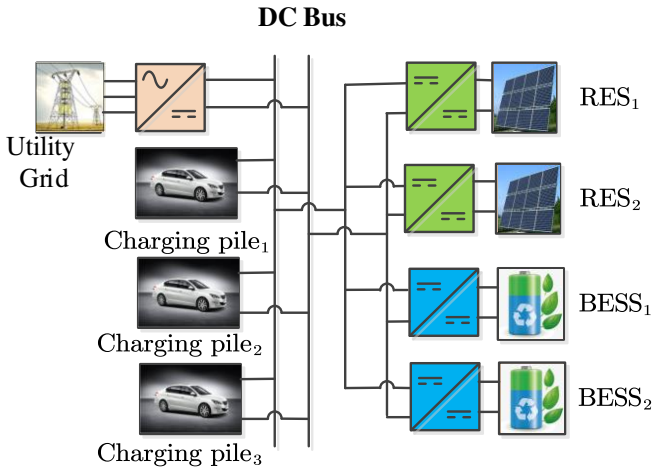

Fig.1 Typical configuration of DC microgrid for EV fast-charging station

II. *The novel SoC-based droop control for BESSs*

A. Design of reference voltage value and droop coefficient

The configuration of the grid-connected DC Microgrid under investigation is illustrated in Fig.2. It consists of a RES unit, a few BESSs, the utility grid and a load, which are all shunt connected to the common DC bus. The BESSs are connected to the DC bus via bidirectional DC-DC converters with line resistance R_{line}. These converters are used for regulating the power flow to and from the DC bus. Power from the utility grid is converted to the DC form via an AC-DC converter connected directly to the DC bus. The utility grid is treated as a power source that is switched on and off according to system requirements; the dynamics of the utility grid power flow are not the focus of this work. Similarly, the RES with its associated DC-DC converter is also treated as a variable power source. The BESSs are the key elements in this system to maintain the DC bus voltage at the required level, while powering the load. There are no communication links between the BESSs, utility grid and RES. The DC bus voltage regulation relies on a flexible SoC-based adaptive V-I droop control scheme for the BESSs and converter units, and its expression is given as

$$V_{bus} = V_{ref} - R_{dr} I \tag{1}$$

where V_{bus} is DC bus voltage filtered by low-pass filter (LPF), V_{ref} is the reference voltage for DC bus, R_{dr} is the droop coefficient, and I is the output current of the DC-DC converter, which is positive when BESS is discharging, negative when BESS is charging. And I_{load} is the current drawn by the load, I_{RES} and I_{grid} are the current from the RES and the utility grid, respectively.

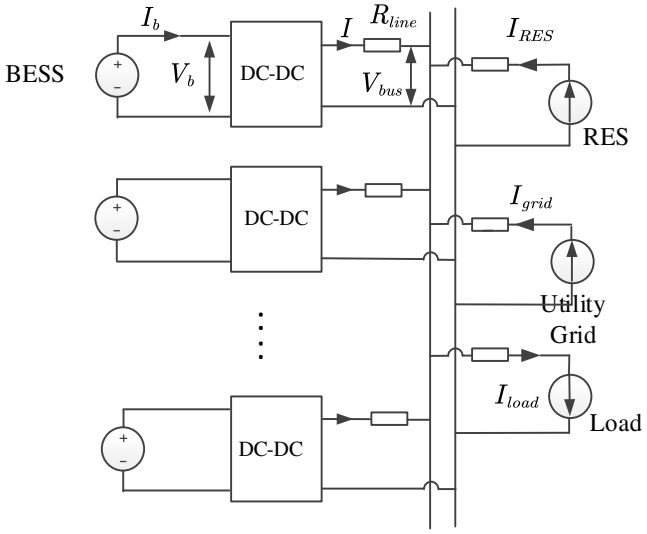

Fig.2 Diagram of DC microgrid with the V-I droop control

A simplified system-level converter model that focuses on the external behavior rather than the internal details is introduced to realize the proposed V-I droop control. Since most converters have current regulating loops or are inherently current source converters, they can be represented as a controllable current source, with the small-signal dynamics represented by a transfer function $G_{conv}(s)$. It has high bandwidth and does not affect the droop control loop [29]. The detailed control algorithm is illustrated in Fig.3.

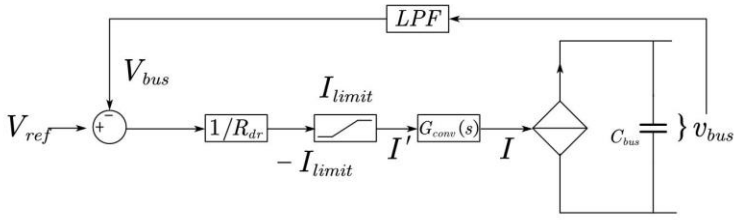

Fig.3 Control algorithm for the V-I droop

The DC bus voltage v_{bus} is processed by a LPF with a cut-off frequency w_c, and transfer function $G_{lpf} = \frac{w_c}{w_c + s}$, then filtered DC bus voltage V_{bus} is compared with V_{ref}, and the error signal divided by the droop coefficient R_{dr} gives the required output current of the DC-DC converter, $\pm I_{limit}$ is the limit for output current of BESS. Thus, with this control loop and neglecting the $G_{conv}(s)$, the output current of the DC-DC converter is given by Eqn (2)

$$I = \frac{V_{ref} - V_{bus}}{R_{dr}} \tag{2}$$

When $V_{ref} > V_{bus}$, BESS is discharging, and when $V_{ref} < V_{bus}$, BESS is charging.

The key requirements in the DC microgrid control with BESS elements are to avoid overcharging or over-discharging of BESSs, while ensuring SoC balance when there are multiple BESSs. To achieve this, the SoC levels for the BESSs need to be included in the V-I droop control law in Eqn (1), and this is done by linking V_{ref} and R_{dr} with the SoC as follows. First, V_{ref} in Eqn (1) is expressed as

$$V_{ref} = \begin{cases} V^*_{ref} + \alpha(SoC - SoC_a) & if\ SoC > SoC_a \\ V^*_{ref} & if\ SoC_a \geq SoC \gg SoC_{min} \\ V_{ref,min} & if\ SoC < SoC_{min} \end{cases} \tag{3a}$$

$$\alpha = \frac{V_{ref,max} - V^*_{ref}}{SoC_{max} - SoC_\alpha} \tag{3b}$$

where $V_{ref,max}$ and $V_{ref,min}$ are, respectively, the upper and lower limits of the reference voltage, V^*_{ref} is the nominal value. These three values are usually determined by the desired DC bus operating range. Similarly, SoC_{max} and SoC_{min} are the upper and low limits of SoC. The control curve of V_{ref} versus SoC is shown in Fig.4. In the normal SoC range, V_{ref} is maintained constant, equal to V^*_{ref}. It increases linearly with SoC when the latter reaches to the high range, which is greater than SoC_α. On the other hand when the SoC reaches its lower limit, V_{ref} is set to $V_{ref,min}$. The benefits of varying V_{ref} are three folds; Firstly, it facilitates that BESSs coordinate utility grid as master units without relying on communication links. By setting V_{ref} to $V_{ref,min}$ when SoC falls to SoC_{min}, V_{bus} becomes low (the relationship between V_{ref} and V_{bus} is shown in Subsection C), this, effectively, informs the utility grid that the SoC is reaching the low limit SoC_{min}, hence utility gird needs to be switched on to inject power to the DC bus and support BESSs. Similarly, when the SoC is higher than SoC_α, V_{ref} increases linearly with SoC according to Eqn (3), resulting, higher V_{bus} which alerts the utility grid controller that the BESSs are in the high SoC range. Correspondingly the utility grid would be switched on to absorb the extra power. Detailed explanations of this coordinated operation will be given in Section III. Secondly, instead of changing V_{ref} with SoC, V_{ref} is maintained to V^*_{ref} while SoC is in the normal operating range. This reduces the variation of V_{bus} which is important for maintaining the stable operation of the DC microgrid. Thirdly, based on the proposed droop control, V_{ref} will be set high when SoC

is in the high range, this allows BESSs discharging more as shown in Eqn (2), hence accelerating the SoC balancing process when multiple BESSs are operating together. This aspect will be further elaborated in Subsection B.

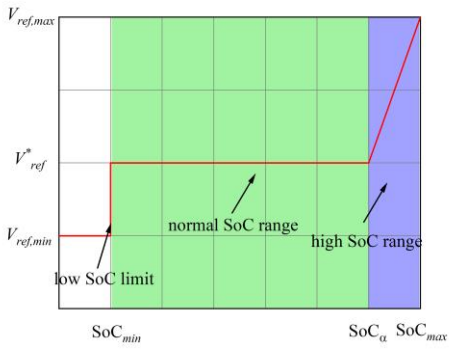

Fig.4 Control curve of V_{ref} versus SoC

Similarly, the droop coefficient R_{dr} is also designed according to the SoC of the BESS, which is expressed as

$$R_{dr} = \begin{cases} k_c SoC^n & I \leq 0 \\ k_d / SoC^n & I > 0 \end{cases} \tag{4}$$

where k_c and k_d are the charging and discharging constants and n is an index for SoC balancing. Setting R_{dr} according to Eqn (4) will facilitate automatic adjusting of charging and discharging speeds [16]. According to Eqn (2), a smaller R_{dr} results in higher BESS charging and discharging currents than a larger R_{dr}. Therefore, in the charging phase, when the BESS with a high SoC value, R_{dr} will take a large value as it is proportional to SoC^n according to Eqn (4), and as a result, the BESS will be charged with smaller current compared with BESS with a low SoC value. On the other hand, in the discharging phase, when the BESS has a high SoC value, since R_{dr} is inversely proportional to SoC^n, R_{dr} will become small, hence the BESS will be discharged with a larger current compared with BESS with low SoC value. Finally, for the BESS with larger power capacity, their corresponding k_c and k_d will be set to smaller values. The details will also be elaborated below Subsection B.

B. SoC balancing study in different scenarios

The proposed voltage droop control enables automatic SoC balancing when multiple BESSs are operating

simultaneously. This can be demonstrated, for the sake of simplicity, using a system with two BESSs (BESS$_i$ and BESS$_j$) with different power capacities W_b and terminal voltages V_b under five different scenarios. With proposed droop control, the charging and discharging currents of BESS$_i$ can be obtained according to Eqn (2) as

$$I_i = \frac{V_{refi} - V_{bus}}{k_{ci} SoC_i^n} \tag{5a}$$

$$I_i = \frac{V_{refi} - V_{bus}}{k_{di}} SoC_i^n \tag{5b}$$

Assuming V_b stays constant within the SoC range from SoC_{min} to SoC_{max}, while the SoC of the BESS can be updated using the coulomb counting method

$$SoC = SoC_0 - \frac{1}{W_b/V_b}\int_0^t i_b dt \tag{6}$$

Where SoC_0 and i_b are, respectively, the initial SoC and output current of BESS. Neglecting the power loss on R_{line} and converter, $i_b = \frac{v_{bus} I}{V_b}$ is obtained. With $i_b = \frac{v_{bus} I}{V_b}$, the ratio of SoC changes for BESS$_i$ and BESS$_j$ derived from Eqn (6) is given as

$$\frac{dSoC_i/dt}{dSoC_j/dt} = \frac{I_i/W_{bi}}{I_j/W_{bj}} \tag{7}$$

If the SoCs of two BESSs are already balanced, then the ratio of SoC changes for the two BESSs defined in (7) to be set to 1 in order to maintain SoC balancing in the subsequent time instants. Substituting Eqn (5) into $\frac{dSoC_i/dt}{dSoC_j/dt} = 1$ yields

$$\frac{k_{ci}}{k_{cj}} = \frac{k_{di}}{k_{dj}} = \frac{W_{bj}}{W_{bi}} \tag{8}$$

Eqn (8) reveals that for the two BESSs, the ratios of their charging and discharging constants are equal to the inversely proportional to their power capacity ratio. Based on this analysis, five scenarios are considered to reveal the dynamics of SoCs balancing with different initial SoCs for the two BESSs.

Scenario 1: $SoC_i > SoC_j$, $V_{refi} = V_{refj} < V_{bus}$, both BESSs are in charging mode.

Substituting Eqn (5a) into Eqn (7) yields

$$\frac{dSoC_i/dt}{dSoC_j/dt} = \frac{(V_{refi} - V_{bus})/(k_{ci} SoC_i^n W_{bi})}{(V_{refj} - V_{bus})/(k_{cj} SoC_j^n W_{bj})} = \frac{SoC_j^n}{SoC_i^n} \tag{9}$$

As $\frac{SoC_j}{SoC_i}<1, \frac{dSoC_i/dt}{dSoC_j/dt}<1$. Eqn (9) implies that the increment change of SoC_j is higher than that of SoC_i, hence SoC_i and SoC_j will be eventually balanced.

Scenario 2: $SoC_i > SoC_j$, $V_{refi} = V_{refj} > V_{bus}$, both BESSs are in discharging mode.

Substituting Eqn (5b) into Eqn (7) yields

$$\frac{dSoC_i/dt}{dSoC_j/dt} = \frac{(V_{refi}-V_{bus})SoC_i^n/(k_{di}W_{bi})}{(V_{refj}-V_{bus})SoC_j^n/(k_{dj}W_{bj})} = \frac{SoC_i^n}{SoC_j^n} \tag{10}$$

As $\frac{SoC_i}{SoC_j}>1, \frac{dSoC_i/dt}{dSoC_j/dt}>1$. Eqn (10) implies that the decrement variation of SoC_i is greater than SoC_j, hence SoC_i and SoC_j will be gradually balanced.

Scenario 3: $SoC_i > SoC_j$, $V_{bus} > V_{refi} > V_{refj}$, both BESSs are in the charging mode.

The ratio of SoC change is expressed as

$$\frac{dSoC_i/dt}{dSoC_j/dt} = \frac{(V_{refi}-V_{bus})/(k_{ci}W_{bi}SoC_i^n)}{(V_{refj}-V_{bus})/(k_{cj}W_{bj}SoC_j^n)} = \frac{V_{refi}-V_{bus}}{V_{refj}-V_{bus}}\frac{SoC_j^n}{SoC_i^n} \tag{11}$$

As $\frac{SoC_j^n}{SoC_i^n}<1$, $\frac{V_{refi}-V_{bus}}{V_{refj}-V_{bus}}<1$, and $\frac{dSoC_i/dt}{dSoC_j/dt}<1$. Eqn (11) implies that the increment variation of SoC_j is higher than SoC_i, hence SoC_i and SoC_j will gradually be balanced.

Scenario 4: $SoC_i > SoC_j$, $V_{refi} > V_{refj} > V_{bus}$, both BESSs are in discharging mode.

The ratio of SoC change is expressed as

$$\frac{dSoC_i/dt}{dSoC_j/dt} = \frac{(V_{refi}-V_{bus})SoC_i^n/(k_{di}W_{bi})}{(V_{refj}-V_{bus})SoC_j^n/(k_{dj}W_{bj})} = \frac{V_{refi}-V_{bus}}{V_{refj}-V_{bus}}\frac{SoC_i^n}{SoC_j^n} \tag{12}$$

As $\frac{SoC_i}{SoC_j}>1$ and $\frac{V_{refi}-V_{bus}}{V_{refj}-V_{bus}}>1, \frac{dSoC_i/dt}{dSoC_j/dt}>1$. Eqn (12) implies that the decrement change of SoC_i is higher than SoC_j, hence SoC_i and SoC_j will be gradually balanced.

Scenario 5: $SoC_i > SoC_j$, $V_{refi} > V_{bus} > V_{refj}$, BESS$_i$ is discharging and BESS$_j$ is charging.

In this scenario, naturally the SoC_i and SoC_j will be eventually balanced.

In the above five scenarios, scenarios 3, 4 and 5 have faster SoC balancing speeds compared to scenarios 1 and 2, this is due to the fact that the difference of V_{ref} between two BESSs helps to accelerate this balancing process. Further, these five scenarios show that index n has an influence on the SoC balancing speed, since

a higher n value leads to a higher ratio of charging or discharging speed between two BESSs. Fig.5 illustrates the balancing process of the two SoCs with n=2 in both BESS charging and discharging modes. Using a constant voltage source injecting or absorbing power to or from the BESSs under the droop control rule (1) while they share the same V_{ref}, it is evident that the difference of SoCs between the two BESSs is reducing exponentially with time, and eventually converges to zero. Fig.6 shows the reduction speed of the SoC difference between the two BESSs with different n. It is clear that a larger n leads to a faster SoC balancing speed in both the charging and discharging phases.

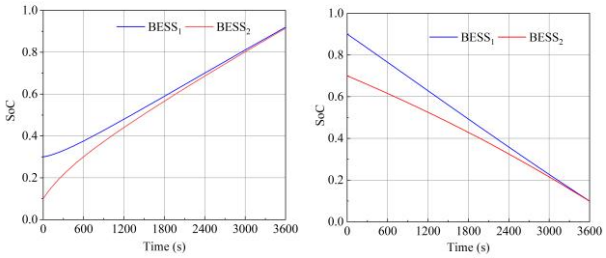

(a) (b)

Fig.5 SoCs of two BESSs obtaining balance with n=2 in (a) charging (b) discharging

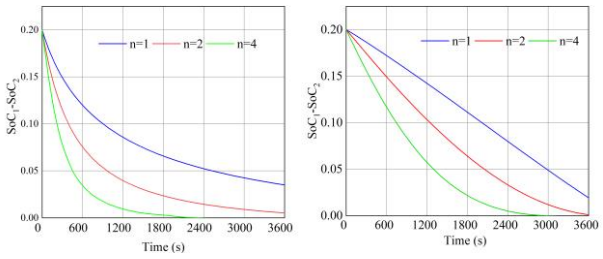

(a) (b)

Fig.6 The difference of SoC between two BESSs with different n in (a) charging (b) discharging

C. Limitations of the control parameters in the proposed SoC-based droop control

To ensure that the variation of V_{bus} is sufficiently small around its nominal value, V_{ref} is set to V_{ref}^{*} when the SoC of a BESS is in the normal range according to Eqn (3). Furthermore, the deviations between V_{bus} and V_{ref} also should be confined to a small range. This requirement consequently sets the limits on the parameters in the proposed droop control and is analyzed below.

As shown in Fig.2, when several BESSs of different capacities are connected in parallel on the DC bus,

their power capacities satisfy the relationships $W_{b1} = \frac{W_{b2}}{\rho_2} = \cdots \frac{W_{bk}}{\rho_k}$. The voltage of the DC bus capacitor C_{bus} can be expressed as

$$V_{bus} = \frac{1}{C_{bus}} \int \sum_{l=1}^{k} I_l - (I_{load} - I_{RES} - I_{grid}) dt \tag{13}$$

Substituting Eqn (2) into Eqn (13) and taking derivative of V_{bus} gives

$$C_{bus} \frac{dV_{bus}}{dt} = \sum_{l=1}^{k} (V_{refl} - V_{bus}) / R_{drl} - (I_{load} - I_{RES} - I_{grid}) \tag{14}$$

When SoCs of the BESSs are balanced, according to Eqn (8), $V_{ref1} = V_{ref2} = \cdots V_{refk} = V_{ref}$, $R_{dr1} = \rho_2 R_{dr2} = \cdots \rho_k R_{drk}$. Subsequently let $K = 1 + \rho_2 + \rho_3 + \cdots \rho_k$, the dynamic of V_{bus} is derived from Eqn (14) and expressed by

$$V_{bus}(t) = (V_{ref} - (I_{load} - I_{RES} - I_{grid}) R_{dr1}/K) \left(1 - exp\left(-\frac{Kt}{C_{bus} R_{dr1}}\right)\right) \tag{15}$$

At the steady-state, the voltage deviation between V_{ref} and V_{bus} can be expressed as

$$\varepsilon = V_{ref} - \lim_{t \to \infty} V_{bus} = (I_{load} - I_{RES} - I_{grid}) R_{dr1}/K \tag{16}$$

where ε is the voltage deviation, which is a small value. Eqn (16) reveals that R_{dr1} must be sufficiently small to ensure a faster response and a smaller voltage deviation range. Assuming allowed maximum $|\varepsilon|$ is δ. The corresponding feasible range for k_{c1} and k_{d1} can be derived from Eqn (16) with δ given as

$$k_{c1} < \frac{K\delta}{(I_{load} - I_{RES} - I_{grid}) SoC^n} \tag{17a}$$

$$k_{d1} < \frac{K\delta SoC^n}{(I_{load} - I_{RES} - I_{grid})} \tag{17b}$$

Apart from the voltage deviation constraint, the power-sharing accuracy between BESSs also needs to be considered. In the conventional droop control [30], only when $R_{dr} \gg R_{line}$ is satisfied, power-sharing accuracy is ensured. However, in the proposed current-source-based droop control, R_{dr} has no influence on the power-sharing accuracy, as elaborated below. Considering R_{line}, the ratio of the output power of BESS$_i$ and BESS$_j$ is expressed by

$$\frac{P_{bi}}{P_{bj}} = \frac{I_i (V_{bus} + I_i R_{linei})}{I_j (V_{bus} + I_j R_{linej})} \tag{18}$$

According to the Kirchhoff current laws (KCL), it holds that

$$I_i + I_j = I_{sum} \tag{19}$$

where $I_{sum} = I_{load} - I_{RES} - I_{grid} - \sum_{l=1}^{k} I_l (l \neq i,j)$

As $V_{refi} = V_{refj}$, substituting Eqn (2) into Eqn (19) yields

$$\frac{I_i}{I_j} = \frac{R_{drj}}{R_{dri}} \tag{20a}$$

$$I_i = \frac{I_{sum}}{1 + R_{dri}/R_{drj}} \tag{20b}$$

$$I_j = \frac{I_{sum}}{1 + R_{drj}/R_{dri}} \tag{20c}$$

As $R_{dri} = R_{dr1}/\rho_i$, $R_{drj} = R_{dr1}/\rho_j$ substituting Eqn (20) into Eqn (18) yields

$$\frac{P_{bi}}{P_{bj}} = \frac{\rho_i}{\rho_j} \frac{V_{bus} + R_{linei} I_{sum}/(1 + \rho_j/\rho_i)}{V_{bus} + R_{linej} I_{sum}/(1 + \rho_i/\rho_j)} \tag{21}$$

The desirable power-sharing between BESS$_i$ and BESS$_j$ is equals to their power capacities ρ_i/ρ_j, thus according to Eqn (21), as long as the inequalities $V_{bus} \gg R_{linei} I_{sum}/(1 + \rho_j/\rho_i)$ and $V_{bus} \gg R_{linej} I_{sum}/(1 + \rho_i/\rho_j)$ are satisfied, the power-sharing accuracy is ensured. More importantly, it is clear that R_{dr} has no influence on the power-sharing accuracy, hence it can be designed independently.

In the microgrid, the SoC operating range is usually set between 0.3-0.9, and $n = 2$ is used in this paper. Although a larger n leads to faster SoC balancing, it causes large voltage variation of ε. Once n is set, Eqn (17) guarantees a feasible range for k_{c1} and k_{d1}, and then, k_{ci} and k_{di} can be calculated as

$$k_{ci} = k_{c1} W_{b1}/W_{bi} \tag{22a}$$

$$k_{di} = k_{d1} W_{b1}/W_{bi} \tag{22b}$$

III. Coordinated operation of the DC microgrid

To fully utilize the power generation capability of RES, it is always desirable to operate renewable generators at their maximum power point (MPP). To regulate the SoCs of BESSs in the microgrid in their operating ranges (avoid overcharging or over-discharging of BESSs), coordinated operation of the utility grid and BESSs is vital. DBS is a widely used decentralized control strategy for DC microgrids due to its simplicity and practicality. It changes the operation mode of utility grid according to V_{bus}. The proposed droop control for the BESSs assisted with DBS realizes the required coordination which is elaborated

below.

Fig.7 illustrates the coordinated operation between BESSs and utility grid at SoC_{min}, which aims to prevent the SoC being lower than SoC_{min}. With preset δ, the possible V_{bus} range when BESS operates between SoC_{min} and SoC_{α} is shown by the blue shading. Thus, if the utility grid detects that V_{bus} is lower than $V_{ref}^{*}-\delta$, which implies that V_{ref} will be set to $V_{ref,min}$ according to Eqn (3) and SoC is lower than SoC_{min}, then the utility grid will be switched on and injects power to charge the BESSs. Similarly, if the utility grid detects that V_{bus} is higher than $V_{ref}^{*}+\delta$, which implies that SoC is slightly higher than SoC_{α}, then utility grid will be switched off.

Fig.8 illustrates the coordinated operation between the BESSs and utility grid in the high SoC range, which aims to prevent charging the BESSs when their SoC is exceeding SoC_{max}. In summary, the utility grid is switched on to absorb power when V_{bus} increases to $V_{ref,max}$, and is switched off when V_{bus} decrease to V^{*}_{ref}. If utility grid detects V_{bus} increases to $V_{ref,max}$, BESSs are charging and V_{ref} satisfies $V_{bus}-\delta<V_{ref}<V_{bus}$, hence V_{ref} is slightly less than $V_{ref,max}$ and SoC is slightly less than SoC_{max}. If V_{bus} decreases to V^{*}_{ref}, BESSs are discharging and V_{ref} satisfies $V_{bus}<V_{ref}<V_{bus}+\delta$, hence V_{ref} is slightly larger than V^{*}_{ref} and SoC is slightly higher than SoC_{α}. As only V_{bus} is the accessible information for estimating SoC of BESSs by the utility grid assisted with the DBS technique, considering that $SoC=(V_{ref}-V_{ref}^{*})/\alpha+SoC_{\alpha}$ in high SoC range, the maximum deviation between V_{ref} and V_{bus} (δ) limits the SoC estimation error within the range of δ/α. Thus, this design enables utility grid to switch on when the SoC is slightly less than SoC_{max} (between $SoC_{max}-\delta/\alpha$ and SoC_{max}) and switch off when the SOC is slightly higher than SoC_{α} (between SoC_{α} and $SoC_{\alpha}+\delta/\alpha$). With these two hysteresis cycles, the coordinated operation of the BESSs and the utility grid can be achieved

As mentioned earlier, with the preset value δ, the grid can not only sense whether the SoC of BESSs reaches SoC_{min}, but also can estimate the SoC within the error limit δ/α when BESSs are in high SoC range, which ensures reliable coordinated operation between the grid and the BESSs.

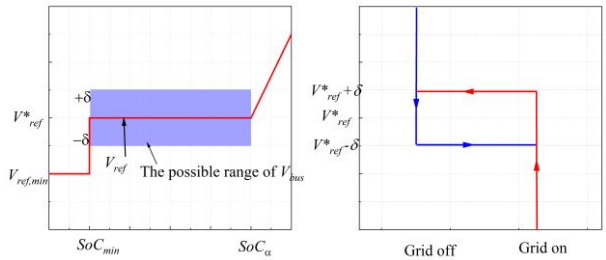

(a) (b)

Fig.7 The coordinated operation between utility grid and BESS at SoC_{min} (a) V_{ref} versus SoC in BESS (b) Utility grid control

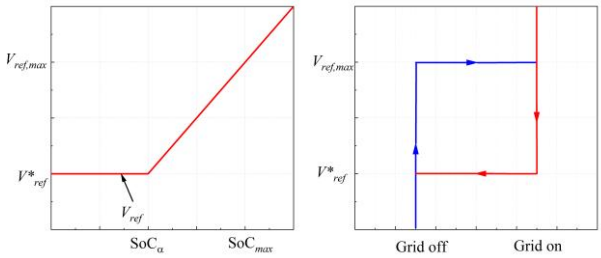

(a) (b)

Fig.8 The coordinated operation between utility grid and BESS in high SoC range (a) V_{ref} versus SoC in BESS (b) Utility grid control

IV. Stability analysis

A. Stability analysis of the DC microgrid with proposed droop control

The stability of the DC microgrid using proposed droop control scheme can be evaluated by applying small-signal analysis. The principle of small-signal analysis is assuming system variables are subject to small disturbances when the system works near the stable operation points, then the system state equation is derived to check if the system is kept stable at small disturbances. The variables x used in the system are expressed as the sum of their steady-state values x_e and small perturbations $\hat{x}$ [21]. The BESS output current I, SoC, and DC bus voltage v_{bus} are taken as variables and perturbed in the following analysis.

Consider the droop curve in Fig.4, the analysis is performed only in the high SoC range since the operation in this range is relatively complicated compared to that in the normal SoC range and low SoC limit. In particular, the control curve in normal SoC range can be viewed as a specific example of high SoC range when $\alpha = 0$, on the other hand, BESSs do not work at low SoC limit, as the utility grid is switched on to

charge BESSs immediately when BESSs fall into low SoC limit.

Neglecting the power losses in converter and line resistances and combing Eqn (6), the SoC of the BESS can be expressed as

$$SoC = SoC_0 - \frac{1}{W_b}\int_0^t v_{bus} I dt \tag{23}$$

In the charging mode when BESSs work at high SoC range, the output current of DC-DC converter is

$$I = \frac{V_{ref}^* + \alpha(SoC - SoC_\alpha) - v_{bus} G_{lpf}}{k_c SoC^n} \tag{24}$$

where G_{lpf} is the transfer function of LPF as shown in Fig.3. Introducing a perturbation to Eqn (24), it yields

$$k_c {SoC_e}^n \hat{I} + n k_c {SoC_e}^{n-1} I_e \hat{SoC} = \alpha \hat{SoC} - G_{lpf} \hat{v_{bus}} \tag{25}$$

Introducing a perturbation to Eqn (23), it yields

$$\hat{SoC} = -\hat{I}\frac{v_{bus\_e}}{W_b s} - \hat{v_{bus}}\frac{I_e}{W_b s} \tag{26}$$

Combing Eqns (25) and (26), we have

$$\hat{I} = \frac{I_e(\alpha - n k_c {SoC_e}^{n-1} I_e) + W_b G_{lpf} s}{(n k_c {SoC_e}^{n-1} I_e - \alpha) v_{bus\_e} - k_c {SoC_e}^n W_b s} \hat{v_{bus}} \tag{27}$$

Considering that RES output current variation $\hat{I_{RES}}$ and grid output current variation $\hat{I_{grid}}$ are neglectable, according to KCL, the current balance equation can be derived as

$$\sum_{i=1}^{k} \frac{I_e(\alpha - n k_{ci} {SoC_{i\_e}}^{n-1} I_{i\_e}) + W_{bi} G_{lpf} s}{(n k_{ci} {SoC_{i\_e}}^{n-1} I_{i-e} - \alpha) v_{bus\_e} - k_{ci} {SoC_{i\_e}}^n W_{bi} s} \hat{v_{bus}} = \frac{\hat{v_{bus}}}{R_{load}} \tag{28}$$

where R_{load} is the equivalent load resistance.

For the sake of simplicity, using a system with two BESSs as an example, expanding Eqn (28) and shifting all terms to the left side, the state equation of DC microgrid at the charging mode can be formulated as

$$A_c s^3 + B_c s^2 + C_c s + D_c = 0 \tag{29}$$

where A_c B_c C_c D_c are provided in Appendix.

Similarly to the charging mode, the output current of DC-DC converter in discharging mode is

$$I = \frac{V_{ref}^{*} + \alpha(SoC - SoC_{\alpha}) - v_{bus}G_{lpf}}{k_d SoC^{-n}} \tag{30}$$

Introducing a perturbation to Eqn (30),

$$k_d SoC_e^{-n} \hat{I} - nk_d SoC_e^{-(n+1)} I_e \hat{SoC} = \alpha \hat{SoC} - G_{lpf} \hat{v}_{bus} \tag{31}$$

Combing Eqn (26) and (31), we have

$$\hat{I} = \frac{I_e(\alpha + nk_d SoC_e^{-(n+1)} I_e) + W_b G_{lpf} s}{(-nk_d SoC_e^{-(n+1)} I_e - \alpha) v_{bus\_e} - k_d SoC_e^{-n} W_b s} \hat{v}_{bus} \tag{32}$$

According to KCL, the current balance equation can be derived as

$$\sum_{i=1}^{k} \frac{I_{i\_e}(\alpha + nk_{di} SoC_{i\_e}^{-(n+1)} I_{i\_e}) + W_{bi} G_{lpf} s}{(-nk_{di} SoC_{i\_e}^{-(n+1)} I_{i\_e} - \alpha) v_{bus\_e} - k_{di} SoC_{i\_e}^{-n} W_{bi} s} \hat{v}_{bus} = \frac{\hat{v}_{bus}}{R_{load}} \tag{33}$$

Expanding Eqn (33) and shifting all terms to the left side, the state equation of DC microgrid at the discharging mode can be formulated as

$$A_d s^3 + B_d s^2 + C_d s + D_d = 0 \tag{34}$$

where A_d B_d C_d D_d are provided in Appendix.

With Eqns (29) and (34), the stability range of DC microgrid are conducted. The influences of k_{c1} and k_{d1} to DC microgrid stability are illustrated in Fig.9 (a) and (b). Assuming $W_{b1} = 2W_{b2}$ and $k_{c2} = 2k_{c1}$, $k_{d2} = 2k_{d1}$, $n = 2$, SoC_{α} is 0.7, SoC_{max} is 0.9, both SoC_{1_e} and SoC_{2_e} are set to 0.8. k_{c1} and k_{d1} increase from 1e-5 to 1 (k_{c2} and k_{d2} also increase accordingly to satisfy $k_{c2} = 2k_{c1}, k_{d2} = 2k_{d1}$), the red and black star represent two different dominant poles for a specific k_{d1}. It is found that all the dominant poles of the DC microgrid system are located in the left half of the s-plane, which confirms that the DC microgrid system is stable with different k_{c1} and k_{d1}. The influence of the SoC value on DC microgrid stability is illustrated in Fig.9 (c) and (d). Assuming $n = 2$, $k_{c2} = 2k_{c1} = 0.02, k_{d2} = 2k_{d1} = 0.02$. SoC_1 keeps equals to SoC_2 and they both increase from 0.7 to 0.9, it is found that all the dominant poles of the DC microgrid are located in the left half of the s-plane when SoC varies from 0.7 to 0.9, which confirms that the DC microgrid is stable within the allowed SoC range.

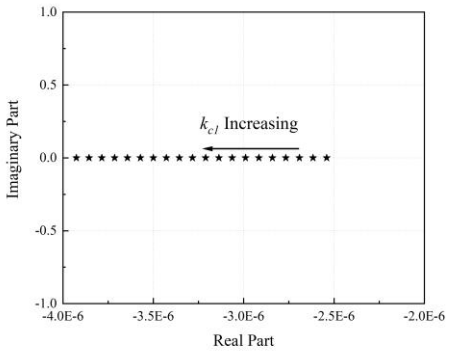

(a) charging with different k_{c1}

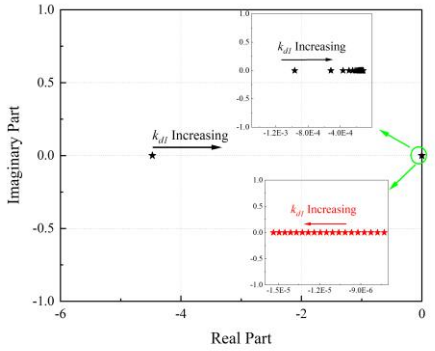

(b) discharging with different k_{d1}

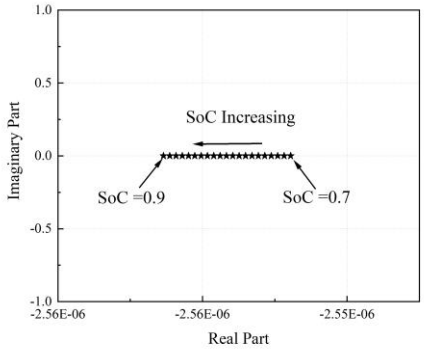

(c) charging with different SoC

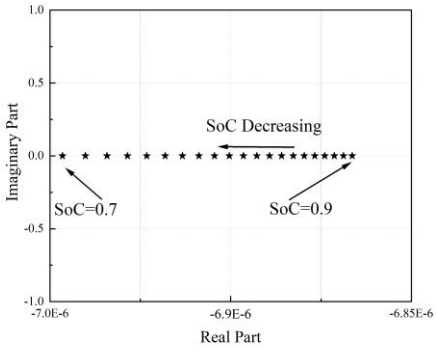

(d) discharging with different SoC

Fig.9 Dominant pole of DC microgrid with proposed droop control

B. Stability analysis of paralleled converters with different loads

To further validate our control strategy, as illustrated in Fig.10, the BESSs are controlled with detailed bi-directional converters and different loads characteristics are considered in the DC microgrid, where the outer control loop for converters is the droop loop which generates reference current I_{ref}, while the inner loop is current loop which tracks the reference current and generates two complementary PWMs for the converters. As the dynamics of the RES and the utility gird are out of the scope of this paper, they are represented by current sources, and the load in the microgrid is categorized into resistive load and constant power load, respectively, where the former is represented by a positive resistance R_{res}, and the latter can be approximated by a negative resistance R_{cpl} and a current source I_{cpl} at the operating point (V_{cpl_e}, I_{cpl_e}), as follows:

$$R_{cpl} = -\frac{{V_{cpl\_e}}^2}{P_{cpl}}$$

$$I_{cpl} = \frac{2P_{cpl}}{V_{cpl\_e}} \tag{35}$$

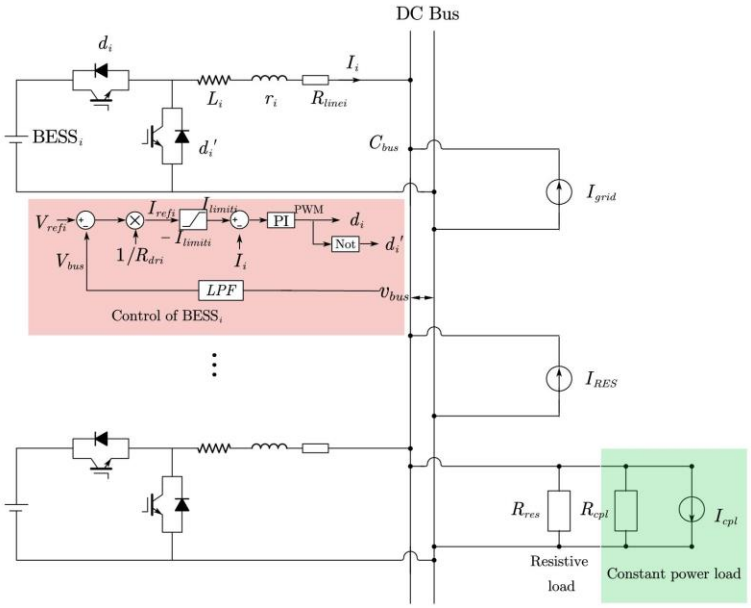

Fig.10 DC microgrid model with paralleled converters and different loads

To analyze the stability of paralleled converters with different loads, we use two paralleled bi-directional converters as an example, and LPF are neglected, based on the average switch model of converters, the stability model based on Fig.10 is illustrated in Fig.11, where $R_{load} = R_{res} \,/\!/\, R_{cpl}$, and the parameters for BESS_1 and BESS_2 are set as follows:

$$V_{b1} = V_{b2} = V_b,\ k_{p1} = k_{p2} = k_p,\ k_{i1} = k_{i2} = k_i,\ L_1 = L_2 = L, r_1 = r_2 = r, R_{line1} = R_{line2} = R_{line}$$

Hence, the state equation based on Fig.11 can be formulated as

$$A_p s^3 + B_p s^2 + C_p s + D_p = 0 \tag{36}$$

where

$$A_p = R_{load} L C_{bus}$$
$$B_p = R_{load} C_{bus} V_b k_p + R_{load} C_{bus} (R_{line} + r) + L$$
$$C_p = R_{load} C_{bus} V_b k_i + R_{load} V_b k_p (1/R_{dr1} + 1/R_{dr2}) + V_b k_p + 2R_{load} + R_{line} + r$$
$$D_p = R_{load} V_b k_i (1/R_{dr1} + 1/R_{dr2}) + V_b k_i$$

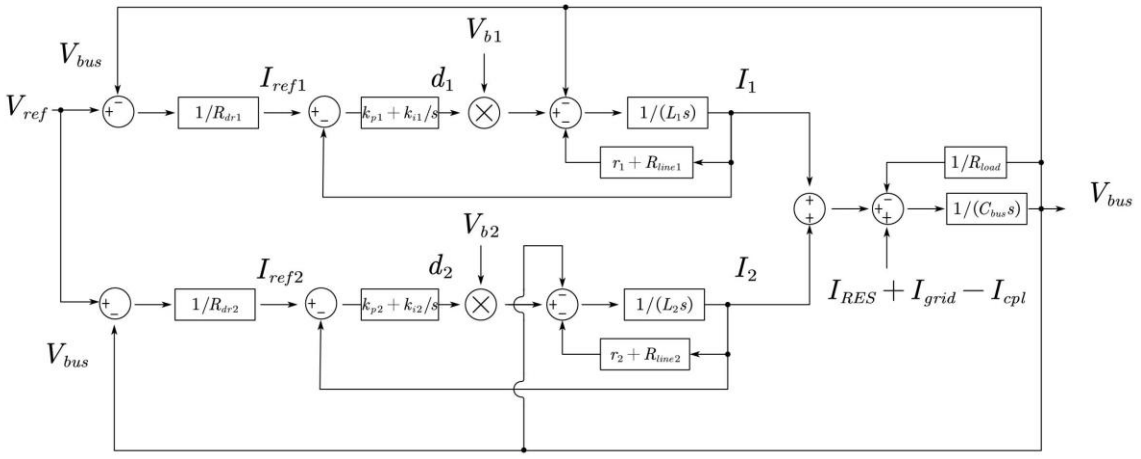

Fig.11 The stability model of paralleled converters with different loads

With Eqn (36), the stability of two paralleled converters with different loads is analyzed. The system is loaded by a resistive load and constant power load, if power of constant power load is lower than resistive load, $|R_{cpl}|>R_{res}$, and $R_{load}>0$, the system is stable when converters are loaded by a positive R_{load}. If power of constant power load is higher than resistive load, $|R_{cpl}|<R_{res}$, then $R_{load}<0$, and system may be unstable with a negative R_{load} [15], thus only the stability with negative R_{load} is analyzed. The influence of R_{load} to paralleled converters stability is illustrated in Fig.12 (a), assuming $R_{dr2}=2R_{dr1}=0.02$, $k_i=10$, $k_p=1$, $V_b=800V$, $V_{ref}=650V$, $C_{bus}=0.1F$, $R_{line}=0.1\Omega$, $r=0.01\Omega$, $L=0.001H$, $|R_{load}|$ decreases from 0.03 to 0.004, the red and black stars in Fig. 12 (a) represent two different dominant poles. It can be seen that the dominant poles approach the right half of the s-plane as $|R_{load}|$ decreases, and the system would be stable only when $|R_{load}|>0.00625$, note that the stability criterion for a buck converter with load is $|R_{load}|>\dfrac{L}{(R_{line}+r)C_{bus}}$ [31], that is $|R_{load}|>0.909$ in this case. Therefore, a smaller $|R_{load}|$ boundary is presented when converters are controlled by the proposed droop control strategy. According to Eqn (35), it allows more constant power load to be plugged into the DC microgrid at a fixed V_{cpl_e}. The influence of R_{dr} to paralleled converters stability is illustrated in Fig 12 (b), assuming $R_{load}=-0.01\Omega$, $R_{dr1}=0.5R_{dr2}$ and R_{dr1} increases from 0.005 to 0.05, other parameters

remain unchanged. It can be seen that the dominant poles approach the right half of the s-plane as R_{dr1} increaseas, the system would become unstable when $R_{dr1} > 0.015$.

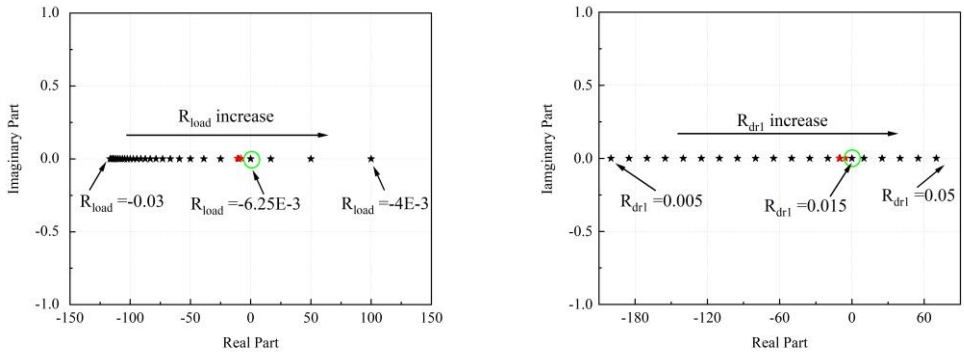

(a) Stability analysis with R_{load} changing (b) Stability analysis with R_{dr1} changing

Fig.12 Dominant poles of parallel converters stability model

V. Hardware-in-loop Results and Discussions

To validate the proposed droop control, the hardware-in-loop (HIL) real-time experiments is conducted at the Typhoon-604 platform and three different scenarios are tested. The HIL experimental set-up is illustrated in Fig.13, where the real-time simulator platform Typhoon HIL604 device shown in the figure has the capability to control the real converters and emulate large power systems in real-time, thus two typhoon HIL604 devices are used in the HIL tests. One device is used as real controller, and the other one is used as a real-time simulator, both the controller and simulator are set up using typhoon's dedicated software in the personal computer. The communication between the controller and real-time simulator is realized through the Ethernet connection interface of the Typhoon HIL604 devices. The first scenario is used to validate the dynamics of the proposed droop control with BESSs mode switching, the second scenario investigates the SoC balancing of three BESSs with the proposed droop control, a 24-hour EV fast charging data set is then used to validate the coordinated operation with the proposed droop control in the third scenario.

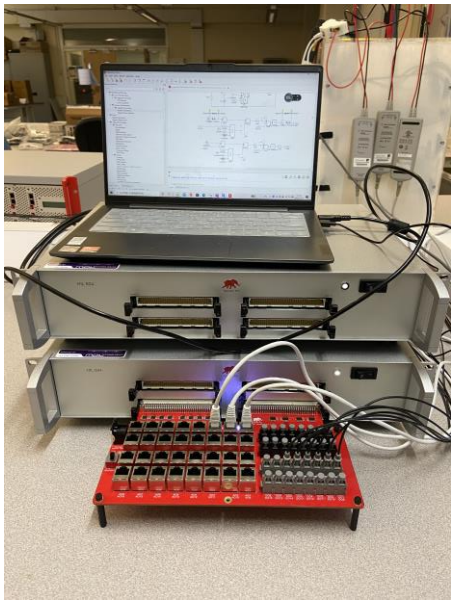

Fig.13 Setup of HIL experiments

A. Dynamic of proposed droop control with BESSs mode switching.

In this scenario, A DC microgrid consists of two BESSs, a RES, the utility grid and a load are used. The control strategy for converters of BESSs is based on Fig.10, and the parameters used in the simulation of Subsection A are given in Table I.

Table I Parameters used in the simulation of Subsection A

Parameters	Value	Parameters	Value
k_{c1}	0.02	V_{ref1}	650V
k_{c2}	0.04	V_{ref2}	650V
k_{d1}	2.5e-3	n	2
k_{d2}	5e-3	C_{bus}	1F
L_i(i=1,2)	1e-2H	I_{limit1}	200A
r_i(i=1,2)	1e-4Ω	I_{limit2}	100A

Assuming the two BESSs have the same SoC values, the dynamics of the proposed droop control with mode switching of BESSs is illustrated in Fig.14. From 0s to 3s, the total current from the external power sources and loads $I_{RES}+I_{grid}-I_{load}$ is 0A, and the initial V_{bus} is 0V due to the large difference between V_{ref} and V_{bus}. Hence, the two BESSs start to discharge with their maximum output current to support the regulation of V_{bus}, and V_{bus} starts to increase linearly with time until it reaches and

stabilizes around 650V eventually. Then, BESSs switch between charging and discharging modes to balance the power mismatch between sources and load, and V_{bus} is stable between mode switching. Furthermore, it can be found that V_{bus} is slightly higher than V_{ref} while BESSs are charging, V_{bus} equals to V_{ref} while BESSs are in idle mode, and V_{bus} is slightly lower than V_{ref} while BESSs are discharging, two BESSs generate or absorb according to their power capacities.

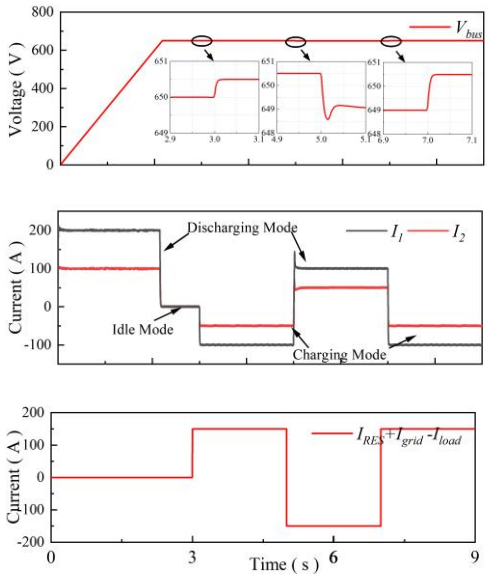

Fig.14 Dynamic of proposed droop control with BESSs mode switching

B. Performance of SoC balance with proposed droop control.

Table II Parameters used in the simulation of Subsection B

Parameters	Value	Parameters	Value
W_{b1}	1300Wh	k_{d2}	5e-3
W_{b2}	650Wh	k_{d3}	5e-3
W_{b3}	650Wh	n	2
k_{c1}	0.02	C_{bus}	1F
k_{c2}	0.04	I_{limit1}	200A
k_{c3}	0.04	I_{limit2}	100A
k_{d1}	2.5e-3	I_{limit3}	100A

In this scenario, three parallelly connected BESSs are adopted, their initial SoCs, namely SoC_1, SoC_2, and SoC_3 are assumed to be 0.8, 0.6, 0.5, respectively. The parameters used in the simulation of Subsection B are shown in Table II, and SoC_α is set 0.7, according to Eqn (3), V_{ref1} is set higher than V_{ref2} and

V_{ref3}. As shown in Fig.15, during the period from 0s to 15s, $I_{RES}+I_{grid}-I_{load}$ is -250A, and three BESSs are in discharging mode to meet the power demand. The SoC balancing is accelerated due to higher V_{ref1}, after about 3s, the reference voltage for $BESS_1$ reaches the same level as the other two BESSs because it starts to work within the normal SoC range ($SoC_1 < SoC_\alpha$), the SoC balancing of these BESSs are achieved through adjusting the droop coefficients. From 15s to 30s, $I_{RES}+I_{grid}-I_{load}$ equals 250A, and the three BESSs switch to the charging mode, and the sudden decrease of R_{dr} implies that the BESSs are switching from the discharging mode to the charging mode. During the charging and discharging of BESSs, the difference of SoCs between the three BESSs is reducing with time, and R_{dr2} and R_{dr3} gradually converge to $2R_{dr1}$, BESSs gradually generate power according to their power capacities.

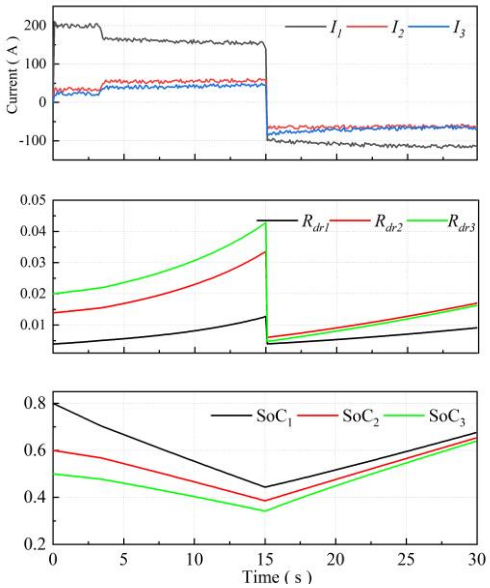

Fig.15 Simulation results of SoC balancing with proposed droop control

C. Performance of coordinated operation of DC microgrid with proposed droop control

To validate the coordinated operation of DC microgrid with proposed droop control, a data set covering 24-hour real-world BESS charging power measured at an EV fast-charging station in Beijing with three charging outlets is used [28]. The configuration of EV fast-charging station is shown in Fig.1, two BESSs, two PVs, utility grid, three piles are connected to DC bus, and three piles act as a load and absorb power. The output powers of PV_1 and PV_2 at the standard weather condition (1000W/m^2, 298.15K) are about 40kW and

30kW, respectively. Fig.16 shows the variations of the solar irradiance on a PV panel over a 24-hour period and the profile of the load charging power in this fast-charging station. To accelerate real-time simulation speed, the initial 24-hour time range data set is compressed 100 times, so the total simulation time is 864s now.

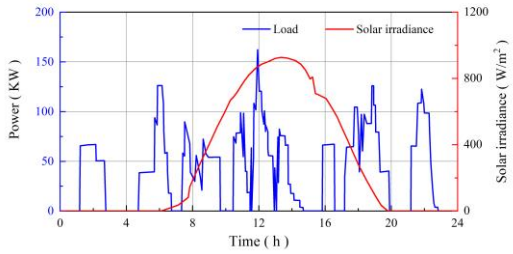

Fig.16 Solar irradiance and load profile in Beijing fast-charging station

Table III The parameters used in the simulation of Subsection C

Parameters	Value	Parameters	Value
W_{b1}	130kWh	SoC_{min}	0.3
W_{b2}	65kWh	SoC_{max}	0.9
k_{c1}	0.018	α	50
k_{c2}	0.036	SoC_{α}	0.7
k_{d1}	2.4e-3	n	2
k_{d2}	4.8e-3	C_{bus}	1F
$V_{ref,min}$	645V	I_{limit1}	200A
$V_{ref,max}$	660V	I_{limit2}	100A

The nominal bus voltage V_{ref}^{*} for EV fast-charging station is set as 650V, and the SoC range for BESSs is set within 0.3-0.9. Although the tolerance limit on the V_{bus} variations in a microgrid is not yet to be standardized [32], a small limit of ±2% of the nominal voltage is adopted, and δ is set as 2.5V, therefore, according to V_{bus} variations requirement and δ constraint, other parameters used in the simulation are obtained and shown in Table III. According to Fig.4, in the high SoC range, the slope, α is 50, hence that δ is 2.5V enables the utility grid to sense the SoC value within 5% (2.5/50) error.

The virtual-battery-model method proposed in [28] is introduced to make a comparison with the proposed method. For a DC microgrid, to maintain the bus voltage within the nominal range is the most critical requirement for system stability, the DC voltage variation range is used as the only criterion for evaluating

the performance of the two methods. Fig.17 shows the variations of V_{bus} using the virtual-battery-model method and the proposed method. In the proposed method, due to the coordinated operation between the BESSs and utility grid, V_{bus} is maintained between 645V and 660V, which are predefined limits $V_{ref,min}$ and $V_{ref,max}$, respectively. Clearly V_{bus} is close to V_{ref}^{*} (650V) for most of the time. Fig.18 illustrates V_{ref} and voltage difference between V_{ref} and V_{bus} (ε), as the SoC of two BESSs is balanced after 50s (shown in Fig.20), only V_{ref} for $BESS_1$ is shown. Furthermore, it is found that ε is constrained smaller than 2.5V.

For the virtual-battery-model method, V_{bus} has similar variation trends which are dependent on the profiles of the solar irradiance and load. However, compared to the results produced by the proposed method, using virtual-battery-model method, V_{bus} exhibits more significant variations. As V_{ref} changes with the SoC in the virtual-battery-model method, it is more fluctuating compared with the proposed method which is kept unchanged when the SoC is within the normal range. To quantify the error between V_{ref}^{*} and V_{bus}, the root-mean-square-error (RMSE) is defined as

$$RMSE = \sqrt{\sum_{i=1}^{N}(V_{ref}^{*} - V_{bus,i})^{2} \Big/ N} \tag{37}$$

where N is the number of measurements. RMSE values for the virtual-battery-model method and the proposed method are 8.7932V and 1.9229V, respectively. It is evident that the latter is significantly smaller, demonstrating better voltage control performance of the proposed method.

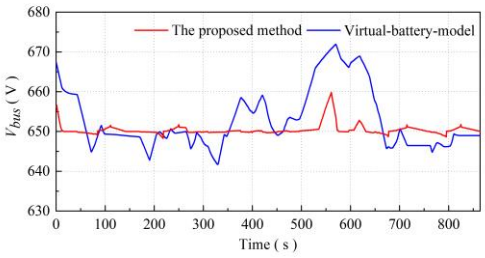

Fig.17 V_{bus} using the proposed method and the virtual-battery-model method

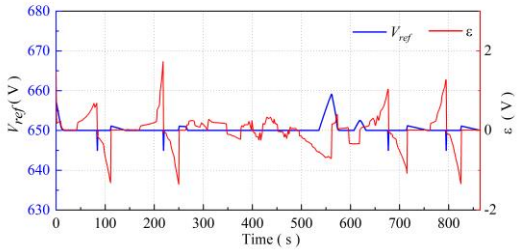

Fig.18 V_{ref} and ε using the proposed method

Fig.19 illustrates the output power of the PV and utility grid obtained with the proposed method. PV always works at the MPPT mode, and the power generation from the PV unit is fully utilized. The solid red line represents the utility grid being switched on to inject power, and the dot red line represents the utility grid being switched on to absorb power. At about 80s, 220s, 670s, and 790s, the SoC reaches its minimal limit SoC_{min}, and the utility grid is switched on to inject power, and at about 550s, the SoC is near its maximal limit SoC_{max}, and the utility grid is switched on to absorb power. The decrease or increase of V_{ref} at these time intervals is shown in Fig.18, which indicates the signals for gird switched on.

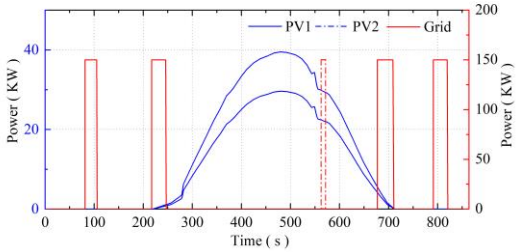

Fig.19 Output power of the PVs and the utility grid

Fig.20 shows the SoC changes of the two BESSs with their initial SoCs of 0.85 and 0.36 respectively. It is shown that they are balanced at around 50s and maintain the same levels in the subsequent hours. Also, they operate at the predefined SoC range of 0.3-0.9 for safety and health purpose. The blue bars in the figure represent the time when the utility grid is switched on to inject power once the SoC drops to SoC_{min} (0.3) and then is switched off when SoC reaches around its predefined value SoC_{α} (0.7). The green bar shows the time when the utility grid is switched on to absorb power once the SoC is near to its upper limit SoC_{max} (0.9) and then is switched off when the SoC decreases to around SoC_{α} (0.7).

Fig.21 illustrates the output current of the two BESSs controlled by the proposed droop control, the output current of $BESS_1$ is the twice of $BESS_2$ when their SoCs are balanced, which implies that the power is shared according to their power capacities. In addition, the output current of the BESS is within its set boundaries $-I_{limit}$ and I_{limit}.

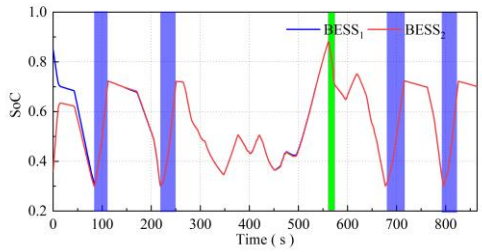

Fig.20 The SoC dynamics of two BESSs

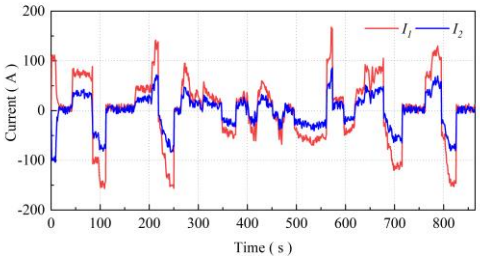

Fig.21 The output Current of the two BESSs

VI. Conclusion

This paper has proposed a novel control strategy for DC microgrids with BESSs without resorting to the communication links. This is achieved by letting the BESSs acting as master units and regulating DC bus voltage with a novel SoC-based droop control, and BESSs coordinate the slave units (e.g. RES, utility grid) to avoid overcharging and over-discharging of the BESSs with the aid of the DC bus signaling (DBS) technique. In the proposed droop control, the reference voltage for BESSs is designed for coordinated operation between BESSs and utility grid, it is maintained constant in the normal SoC range, unless the BESS reaches its low SoC limit or lies in the high SoC range, which reduces DC bus voltage variation; droop coefficients are designed for SoC balance, they are adjusted dynamically based on their own SoC values of the BESSs. Furthermore, the preset maximum deviation between the reference voltage and DC bus voltage ensures reliable coordinated operation between BESSs and utility grid. That BESSs act as master units helps RES generates maximum power and DC microgrid work autonomously (in islanded mode) in most of time. Since the proposed droop controller is current source-based, the droop coefficients do not affect power-sharing accuracy, hence when determining droop coefficients it does not have a trade-off between voltage regulation and power-sharing accuracy like many conventional methods. Finally, the real-time HIL simulation experiments have validated the effectiveness of the proposed method with three different scenarios.

Comparisons of the proposed method with the popular virtual-battery-model method confirm the efficacy and superiority of the proposed control method.

Considering the health and output characteristics of batteries, they are often used to compensate the low-frequency power fluctuations in the microgrid, and high-frequency power fluctuations are compensated by supercapacitors. Besides the frequency of power fluctuations, the degradation costs of multiple batteries and supercapacitors also should be considered in the power-sharing among these different energy storage devices. To investigate the power fluctuation frequency and degradation costs of energy storage devices based power-sharing strategy for hybrid energy storage systems will be a future work. In our previous work, we have introduced a constrained optimization framework for charging and discharging control of batteries [33][34][35] which could incorporate multiple objectives including the degradation costs. More specifically, from the manufacturer's datasheet, the battery theoretic life cycle with depth of discharge (DoD) can be obtained. Since DoD=1-SoC, the incremental battery degradation cost (IBDC) with SoC variation changing can be timely updated while the battery is charging or discharging. Then droop coefficient for each battery can be adjusted according to the IBDC, where higher droop coefficient leads to lower charging or discharging current. Therefore, the battery with a higher IBDC will adopt a higher droop coefficient both in charging mode and discharging mode. This principle can be incorporated into the future power sharing controller design.

Acknowledgments

The work is partially supported by SP Energy Networks on the project 'A holistic approach for power system monitoring to support DSO transition' and EPSRC funded project on 'Creating Resilient Sustainable Microgrids through Hybrid Renewable Energy Systems' under grant EP/R030243/1.

Jialei SU would like to thank the China Scholarship Council for the financial support of his PhD study at University of Leeds

Reference

[1] D. E. Olivares *et al.*, "Trends in microgrid control," *IEEE Transactions on Smart Grid,* Article vol. 5, no. 4, pp. 1905-1919, 2014, Art. no. 6818494.

[2] A. A. R. Lasseter, C. Marnay, J. Stevens, J. Dagle, R. Guttromson, A. Meliopoulous, R. Yinger, and J. Oto, "The certs microgrid concept—White paper on integration of distributed energy resources," *U.S. Dept. Energy, Lawrence Berkeley Nat. Lab., Berkeley, CA, USA, Tech. Rep.LBNL-50829,* 2002.

[3] Y. Wang, D. Liu, P. Liu, F. Deng, D. Zhou, and Z. Chen, "Lifetime-Oriented Droop Control Strategy for AC Islanded Microgrids," *IEEE Transactions on Industry Applications,* vol. 55, no. 3, pp. 3252-3263, 2019.

[4] B. Adineh, R. Keypour, P. Davari, and F. Blaabjerg, "Review of Harmonic Mitigation Methods in Microgrid: From a Hierarchical Control Perspective," *IEEE Journal of Emerging and Selected Topics in Power Electronics,* vol. 9, no. 3, pp. 3044-3060, 2021.

[5] M. Raza, C. Collados, and O. Gomis-Bellmunt, "Reactive power management in an offshore AC network having multiple voltage source converters," *Applied Energy,* Article vol. 206, pp. 793-803, 2017.

[6] M. Ashabani, H. B. Gooi, and J. M. Guerrero, "Designing high-order power-source synchronous current converters for islanded and grid-connected microgrids," *Applied Energy,* Article vol. 219, pp. 370-384, 2018.

[7] T. Dragicevic, J. M. Guerrero, J. C. Vasquez, and D. Skrlec, "Supervisory control of an adaptive-droop regulated DC microgrid with battery management capability," *IEEE Transactions on Power Electronics,* vol. 29, no. 2, pp. 695-706, 2014, Art. no. 6497633.

[8] R. H. Ashique, Z. Salam, M. J. Bin Abdul Aziz, and A. R. Bhatti, "Integrated photovoltaic-grid dc fast charging system for electric vehicle: A review of the architecture and control," *Renewable and Sustainable Energy Reviews,* vol. 69, pp. 1243-1257, 2017.

[9] C. Jin, P. Wang, J. Xiao, Y. Tang, and F. H. Choo, "Implementation of hierarchical control in DC microgrids," *IEEE Transactions on Industrial Electronics,* vol. 61, no. 8, pp. 4032-4042, 2014, Art. no. 6642055.

[10] S. Parhizi, H. Lotfi, A. Khodaei, and S. Bahramirad, "State of the art in research on microgrids: A review," *IEEE Access,* Review vol. 3, pp. 890-925, 2015, Art. no. 07120901.

[11] P. Singh, P. Paliwal, and A. Arya, "A Review on Challenges and Techniques for Secondary Control of Microgrid," in *IOP Conference Series: Materials Science and Engineering*, 2019, vol. 561.

[12] C. Gavriluta, I. Candela, C. Citro, A. Luna, and P. Rodriguez, "Decentralized control of MTDC networks with energy storage and distributed generation," in *2013 IEEE Energy Conversion Congress and Exposition, ECCE 2013*, 2013, pp. 2657-2663.

[13] N. L. Díaz, A. C. Luna, J. C. Vasquez, and J. M. Guerrero, "Centralized Control Architecture for Coordination of Distributed Renewable Generation and Energy Storage in Islanded AC Microgrids," *IEEE Transactions on Power Electronics,* Article vol. 32, no. 7, pp. 5202-5213, 2017, Art. no. 7564412.

[14] K. T. Tan, X. Y. Peng, P. L. So, Y. C. Chu, and M. Z. Q. Chen, "Centralized control for parallel operation of distributed generation inverters in microgrids," *IEEE Transactions on Smart Grid,* Article vol. 3, no. 4, pp. 1977-1987, 2012, Art. no. 6268310.

[15] T. Dragicevic, X. Lu, J. C. Vasquez, and J. M. Guerrero, "DC Microgrids - Part I: A Review of

Control Strategies and Stabilization Techniques," *IEEE Transactions on Power Electronics,* vol. 31, no. 7, pp. 4876-4891, 2016, Art. no. 7268934.

[16] X. Lu, K. Sun, J. M. Guerrero, J. C. Vasquez, and L. Huang, "Double-quadrant state-of-charge-based droop control method for distributed energy storage systems in autonomous DC Microgrids," *IEEE Transactions on Smart Grid,* Article vol. 6, no. 1, pp. 147-157, 2015, Art. no. A29.

[17] X. Lu, K. Sun, J. M. Guerrero, J. C. Vasquez, and L. Huang, "State-of-charge balance using adaptive droop control for distributed energy storage systems in DC microgrid applications," *IEEE Transactions on Industrial Electronics,* Article vol. 61, no. 6, pp. 2804-2815, 2014, Art. no. 6584748.

[18] Y. Mi *et al.*, "The coordinated control strategy for isolated DC microgrid based on adaptive storage adjustment without communication," *Applied Energy,* vol. 252, 2019, Art. no. 113465.

[19] Y. Zeng *et al.*, "State-of-charge dynamic balancing strategy for distributed energy storage system in DC shipboard microgrid," *International Journal of Electrical Power & Energy Systems,* vol. 133, p. 107094, 2021/12/01/ 2021.

[20] Q. Yang, L. Jiang, H. Zhao, and H. Zeng, "Autonomous Voltage Regulation and Current Sharing in Islanded Multi-Inverter DC Microgrid," *IEEE Transactions on Smart Grid,* vol. 9, no. 6, pp. 6429-6437, 2018.

[21] N. Zhi, K. Ding, L. Du, and H. Zhang, "An SOC-Based Virtual DC Machine Control for Distributed Storage Systems in DC Microgrids," *IEEE Transactions on Energy Conversion,* Article vol. 35, no. 3, pp. 1411-1420, 2020, Art. no. 9003422.

[22] C. Zhang, P. Li, and Y. Guo, "Bidirectional DC/DC and SOC Drooping Control for DC Microgrid Application," *Electronics,* vol. 9, no. 2, 2020.

[23] J. Lee, Y. Kim, T. Kim, and S. Moon, "Novel Droop Control of Battery Energy Storage Systems Based on Battery Degradation Cost in Islanded DC Microgrids," *IEEE Access,* vol. 8, pp. 119337-119345, 2020.

[24] Z. Shuai, J. Fang, F. Ning, and Z. J. Shen, "Hierarchical structure and bus voltage control of DC microgrid," *Renewable and Sustainable Energy Reviews,* Review vol. 82, pp. 3670-3682, 2018.

[25] D. Wu, F. Tang, T. Dragicevic, J. M. Guerrero, and J. C. Vasquez, "Coordinated control based on bus-signaling and virtual inertia for Islanded DC Microgrids," *IEEE Transactions on Smart Grid,* vol. 6, no. 6, pp. 2627-2638, 2015, Art. no. 7015592.

[26] P. García-Triviño, J. P. Torreglosa, L. M. Fernández-Ramírez, and F. Jurado, "Control and operation of power sources in a medium-voltage direct-current microgrid for an electric vehicle fast charging station with a photovoltaic and a battery energy storage system," *Energy,* vol. 115, pp. 38-48, 2016.

[27] Y. Xia, M. Yu, P. Yang, Y. Peng, and W. Wei, "Generation-Storage Coordination for Islanded DC Microgrids Dominated by PV Generators," *IEEE Transactions on Energy Conversion,* Article vol. 34, no. 1, pp. 130-138, 2019, Art. no. 8421035.

[28] S. Wang, L. Lu, X. Han, M. Ouyang, and X. Feng, "Virtual-battery based droop control and energy storage system size optimization of a DC microgrid for electric vehicle fast charging station," *Applied Energy,* Article vol. 259, 2020, Art. no. 114146.

[29] Y. Gu, X. Xiang, W. Li, and X. He, "Mode-adaptive decentralized control for renewable DC microgrid with enhanced reliability and flexibility," *IEEE Transactions on Power Electronics,* vol. 29, no. 9, pp. 5072-5080, 2014, Art. no. 6678794.

[30] X. Lu, J. M. Guerrero, K. Sun, and J. C. Vasquez, "An Improved Droop Control Method for DC Microgrids Based on Low Bandwidth Communication With DC Bus Voltage Restoration and Enhanced Current Sharing Accuracy," *IEEE Transactions on Power Electronics,* vol. 29, no. 4, pp. 1800-1812, 2014.

[31] A. M. Rahimi and A. Emadi, "Active Damping in DC/DC Power Electronic Converters: A Novel Method to Overcome the Problems of Constant Power Loads," *IEEE Transactions on Industrial Electronics,* vol. 56, no. 5, pp. 1428-1439, 2009.

[32] M. N. Hussain, R. Mishra, and V. Agarwal, "A Frequency-Dependent Virtual Impedance for Voltage-Regulating Converters Feeding Constant Power Loads in a DC Microgrid," *IEEE Transactions on Industry Applications,* Article vol. 54, no. 6, pp. 5630-5639, 2018, Art. no. 8382321.

[33] K. Liu, K. Li, C. Zhang, "Constrained generalized predictive control of battery charging process based on a coupled thermoelectric model', Journal of Power Sources, Vol. 347, pp.145-158, 2017.

[34] K. Liu, K. Li, H. Ma, J. Zhang, Q. Peng, "Multi-objective optimization of charging patterns for lithium-ion battery management", Energy Conversion and Management, Vol. 159, pp. 151-162, 2018.

[35] K. Liu, C. Zou, K. Li and T. Wik, "Charging Pattern Optimization for Lithium-Ion Batteries With an Electrothermal-Aging Model," in IEEE Transactions on Industrial Informatics, vol. 14, no. 12, pp. 5463-5474, Dec. 2018.

APPENDIX

$$A_c = -k_{c1}k_{c2}W_{b1}W_{b2}SoC_{1\_e}^{n}SoC_{2\_e}^{n}$$

$$B_c = -w_c k_{c1}k_{c2}W_{b1}W_{b2}SoC_{1\_e}^{n}SoC_{2\_e}^{n} - R_{load}w_c W_{b1}W_{b2}(k_{c1}SoC_{1\_e}^{n} + k_{c2}SoC_{2\_e}^{n}) + k_{c2}W_{b2}SoC_{2\_e}^{n}(nk_{c1}SoC_{1\_e}^{n-1}I_{1\_e}v_{bus\_e} - \alpha v_{bus\_e})$$
$$- R_{load}(k_{c2}W_{b2}SoC_{2\_e}^{n}(\alpha I_{1\_e} - nk_{c1}SoC_{1\_e}^{n-1}I_{1\_e}{}^{2}) + k_{c1}W_{b1}SoC_{1\_e}^{n}(\alpha I_{2\_e} - nk_{c2}SoC_{2\_e}^{n-1}I_{2\_e}{}^{2})) + k_{c1}W_{b1}SoC_{1\_e}^{n}(nk_{c2}SoC_{2\_e}^{n-1}I_{2\_e}v_{bus\_e} - \alpha v_{bus\_e})$$

$$C_c = -R_{load}w_c(k_{c2}W_{b2}SoC_{2\_e}^{n}(\alpha I_{1\_e} - nk_{c1}SoC_{1\_e}^{n-1}I_{1\_e}{}^{2}) + k_{c1}W_{b1}SoC_{1\_e}^{n}(\alpha I_{2\_e} - nk_{c2}SoC_{2\_e}^{n-1}I_{2\_e}{}^{2})) + w_c k_{c2}W_{b2}SoC_{2\_e}^{n}(nk_{c1}SoC_{1\_e}^{n-1}I_{1\_e}v_{bus\_e} - \alpha v_{bus\_e})$$
$$+ w_c k_{c1}W_{b1}SoC_{1\_e}^{n}(nk_{c2}SoC_{2\_e}^{n-1}I_{2\_e}v_{bus\_e} - \alpha v_{bus\_e}) + R_{load}w_c W_{b2}(nk_{c1}SoC_{1\_e}^{n-1}I_{1\_e}v_{bus\_e} - \alpha v_{bus\_e}) + R_{load}w_c W_{b1}(nk_{c2}SoC_{2\_e}^{n-1}I_{2\_e}v_{bus\_e} - \alpha v_{bus\_e})$$
$$+ R_{load}(nk_{c2}SoC_{2\_e}^{n-1}I_{2\_e}v_{bus\_e} - \alpha v_{bus\_e})(\alpha I_{1\_e} - nk_{c1}SoC_{1\_e}^{n-1}I_{1\_e}{}^{2}) + R_{load}(\alpha I_{2\_e} - nk_{c2}SoC_{2\_e}^{n-1}I_{2\_e}{}^{2})(nk_{c1}SoC_{1\_e}^{n-1}I_{1\_e}v_{bus\_e} - \alpha v_{bus\_e})$$
$$- (nk_{c1}SoC_{1\_e}^{n-1}I_{1\_e}v_{bus\_e} - \alpha v_{bus\_e})(nk_{c2}SoC_{2\_e}^{n-1}I_{2\_e}v_{bus\_e} - \alpha v_{bus\_e})$$

$$D_c = R_{load}w_c(\alpha I_{1\_e} - nk_{c1}SoC_{1\_e}^{n-1}I_{1\_e}{}^{2})(nk_{c2}SoC_{2\_e}^{n-1}I_{2\_e}v_{bus\_e} - \alpha v_{bus\_e}) + R_{load}w_c(\alpha I_{2\_e} - nk_{c2}SoC_{2\_e}^{n-1}I_{2\_e}{}^{2})(nk_{c1}SoC_{1\_e}^{n-1}I_{1\_e}v_{bus\_e} - \alpha v_{bus\_e})$$
$$- w_c(nk_{c1}SoC_{1\_e}^{n-1}I_{1\_e}v_{bus\_e} - \alpha v_{bus\_e})(nk_{c2}SoC_{2\_e}^{n-1}I_{2\_e}v_{bus\_e} - \alpha v_{bus\_e})$$

$$A_d = -k_{d1}k_{d2}W_{b1}W_{b2}SoC_{1\_e}^{-n}SoC_{2\_e}^{-n}$$

$$B_d = -w_c k_{d1}k_{d2}W_{b1}W_{b2}SoC_{1\_e}^{-n}SoC_{2\_e}^{-n} - R_{load}w_c W_{b1}W_{b2}(k_{d1}SoC_{1\_e}^{-n} + k_{d2}SoC_{2\_e}^{-n}) + k_{d2}W_{b2}SoC_{2\_e}^{-n}(-nk_{d1}SoC_{1\_e}^{-(n+1)}I_{1\_e}v_{bus\_e} - \alpha v_{bus\_e})$$
$$- R_{load}(k_{d2}W_{b2}SoC_{2\_e}^{-n}(\alpha I_{1\_e} + nk_{d1}SoC_{1\_e}^{-(n+1)}I_{1\_e}{}^{2}) + k_{d1}W_{b1}SoC_{1\_e}^{-n}(\alpha I_{2\_e} + nk_{d2}SoC_{2\_e}^{-(n+1)}I_{2\_e}{}^{2})) + k_{d1}W_{b1}SoC_{1\_e}^{-n}(-nk_{d2}SoC_{2\_e}^{-(n+1)}I_{2\_e}v_{bus\_e} - \alpha v_{bus\_e})$$

$$C_d = -R_{load} w_c \left(k_{d2} W_{b2} SoC_{2\_e}^{-n} \left(\alpha I_{1\_e} + n k_{d1} SoC_{1\_e}^{-(n+1)} {I_{1\_e}}^2\right) + k_{d1} W_{b1} SoC_{1\_e}^{n} \left(\alpha I_{2\_e} + n k_{d2} SoC_{2\_e}^{-(n+1)} {I_{2\_e}}^2\right)\right)$$
$$+ w_c k_{d1} W_{b1} SoC_{1\_e}^{-n} \left(-n k_{d2} SoC_{2\_e}^{-(n+1)} I_{2\_e} v_{bus\_e} - \alpha v_{bus\_e}\right) + R_{load} w_c W_{b2} \left(-n k_{d1} SoC_{1\_e}^{-(n+1)} I_{1\_e} v_{bus\_e} - \alpha v_{bus\_e}\right) + R_{load} w_c W_{b1} \left(-n k_{d2} SoC_{2\_e}^{-(n+1)} I_{2\_e} v_{bus\_e} - \alpha v_{bus\_e}\right)$$
$$+ R_{load} \left(-n k_{d2} SoC_{2\_e}^{-(n+1)} I_{2\_e} v_{bus\_e} - \alpha v_{bus\_e}\right) \left(\alpha I_{1\_e} + n k_{d1} SoC_{1\_e}^{-(n+1)} {I_{1\_e}}^2\right) + R_{load} \left(\alpha I_{2\_e} + n k_{d2} SoC_{2\_e}^{-(n+1)} {I_{2\_e}}^2\right) \left(-n k_{d1} SoC_{1\_e}^{-(n+1)} I_{1\_e} v_{bus\_e} - \alpha v_{bus\_e}\right)$$
$$- \left(n k_{d1} SoC_{1\_e}^{-(n+1)} I_{1\_e} v_{bus\_e} + \alpha v_{bus\_e}\right) \left(n k_{d2} SoC_{2\_e}^{-(n+1)} I_{2\_e} v_{bus\_e} + \alpha v_{bus\_e}\right) + w_c k_{d2} W_{b2} SoC_{2\_e}^{-n} \left(-n k_{d1} SoC_{1\_e}^{-(n+1)} I_{1\_e} v_{bus\_e} - \alpha v_{bus\_e}\right)$$
$$D_d = R_{load} w_c \left(\alpha I_{1\_e} + n k_{d1} SoC_{1\_e}^{-(n+1)} {I_{1\_e}}^2\right) \left(-n k_{d2} SoC_{2\_e}^{-(n+1)} I_{2\_e} v_{bus\_e} - \alpha v_{bus\_e}\right) + R_{load} w_c \left(\alpha I_{2\_e} + n k_{d2} SoC_{2\_e}^{-(n+1)} {I_{2\_e}}^2\right) \left(-n k_{d1} SoC_{1\_e}^{-(n+1)} I_{1\_e} v_{bus\_e} - \alpha v_{bus\_e}\right)$$
$$- w_c \left(n k_{d1} SoC_{1\_e}^{-(n+1)} I_{1\_e} v_{bus\_e} + \alpha v_{bus\_e}\right) \left(n k_{d2} SoC_{2\_e}^{-(n+1)} I_{2\_e} v_{bus\_e} + \alpha v_{bus\_e}\right)$$